Restoration of the defect in radial glial fiber migration and cortical plate organization in a brain organoid model of Fukuyama muscular dystrophy

Taniguchi-Ikeda, Mariko ; Koyanagi-Aoi, Michiyo ; Maruyama, Tatsuo ; Takaori, Toru ; Hosoya, Akiko ; Tezuka, Hiroyuki ; Nagase, Shotaro ;…

(Citation)
iScience,24(10):103140

(Issue Date)
2021-10-22

(Resource Type)
journal article

(Version)
Version of Record

(URL)
https://hdl.handle.net/20.500.14094/90008795

iScience

CellPress
OPEN ACCESS

Article

Restoration of the defect in radial glial fiber migration and cortical plate organization in a brain organoid model of Fukuyama muscular dystrophy

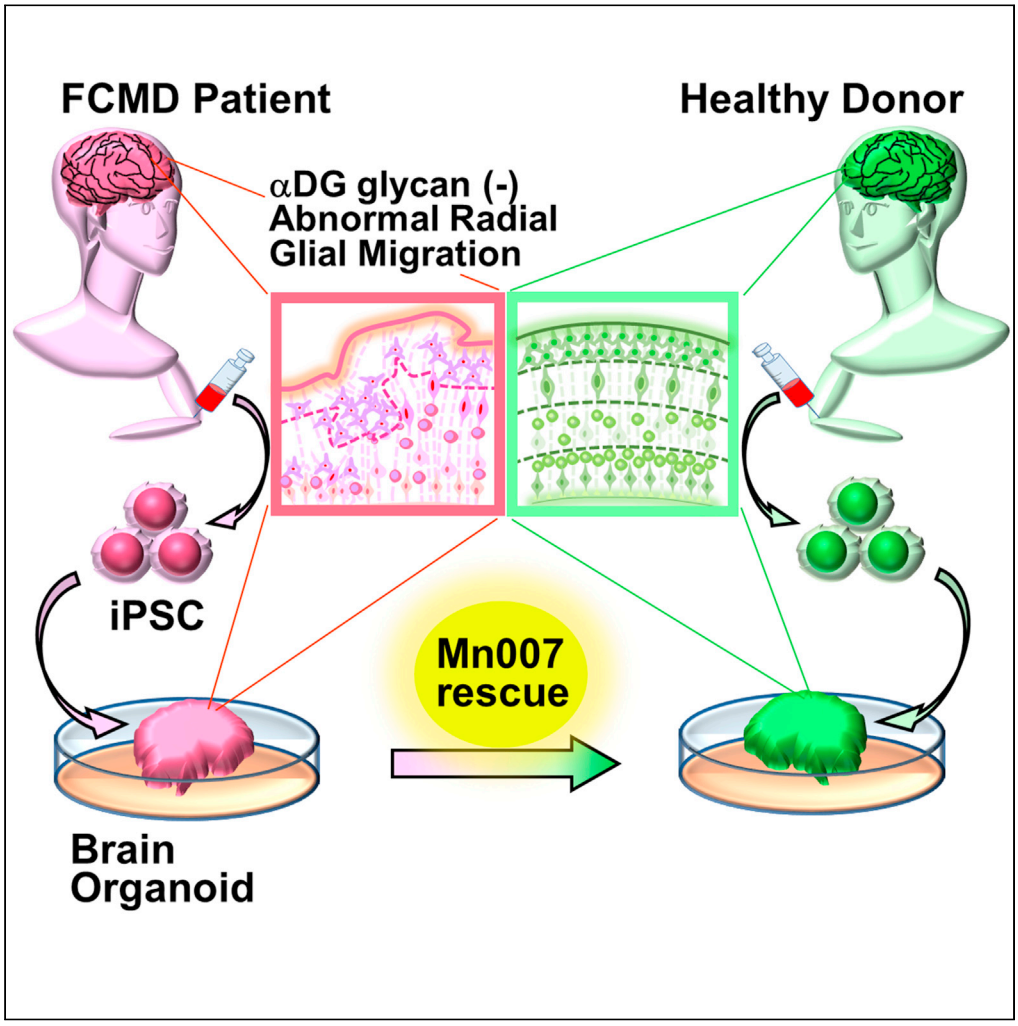

Mariko Taniguchi-Ikeda, Michiyo Koyanagi-Aoi, Tatsuo Maruyama, ..., Tatsushi Toda, Momoko Watanabe, Takashi Aoi

mtani@fujita-hu.ac.jp

Highlights

FCMD muscle and brain defects result from reduced α-dystroglycan (α-DG) glycosylation

iPSC-derived brain organoids exhibit structural defects like those seen in FCMD patients

FCMD organoids exhibit decreased α-DG glycosylation and abnormal radial glial migrations

Mannan-007 partially restored α-DG glycosylation and radial glial migration defects

Taniguchi-Ikeda et al., iScience 24, 103140 October 22, 2021
https://doi.org/10.1016/j.isci.2021.103140

iScience

CellPress
OPEN ACCESS

Article

Restoration of the defect in radial glial fiber migration and cortical plate organization in a brain organoid model of Fukuyama muscular dystrophy

Mariko Taniguchi-Ikeda,[1,2,3,23,*] Michiyo Koyanagi-Aoi,[4,5,6] Tatsuo Maruyama,[7] Toru Takaori,[8,9] Akiko Hosoya,[4,5,6] Hiroyuki Tezuka,[10] Shotaro Nagase,[11] Takuma Ishihara,[12] Taisuke Kadoshima,[11] Keiko Muguruma,[13,14] Keiko Ishigaki,[15] Hidetoshi Sakurai,[8] Akira Mizoguchi,[16] Bennett G. Novitch,[17,18,19] Tatsushi Toda,[20] Momoko Watanabe,[21,22] and Takashi Aoi[4,5,6]

SUMMARY

Fukuyama congenital muscular dystrophy (FCMD) is a severe, intractable genetic disease that affects the skeletal muscle, eyes, and brain and is attributed to a defect in alpha dystroglycan (αDG) *O*-mannosyl glycosylation. We previously established disease models of FCMD; however, they did not fully recapitulate the phenotypes observed in human patients. In this study, we generated induced pluripotent stem cells (iPSCs) from a human FCMD patient and differentiated these cells into three-dimensional brain organoids and skeletal muscle. The brain organoids successfully mimicked patient phenotypes not reliably reproduced by existing models, including decreased αDG glycosylation and abnormal radial glial (RG) fiber migration. The basic polycyclic compound Mannan-007 (Mn007) restored αDG glycosylation in the brain and muscle models tested and partially rescued the abnormal RG fiber migration observed in cortical organoids. Therefore, our study underscores the importance of αDG *O*-mannosyl glycans for normal RG fiber architecture and proper neuronal migration in corticogenesis.

INTRODUCTION

Fukuyama congenital muscular dystrophy (FCMD) is a severe neuromuscular genetic disorder affecting the eyes, brain, and muscles that is categorized as muscular dystrophy-dystroglycanopathy type A4 (MIM 253800; (Fukuyama et al., 1981)). FCMD is classified as an α-dystroglycanopathy (αDGpathy) because it is invariably caused by gene mutations associated with the *O*-mannose glycosylation of α-dystroglycan (αDG; (Muntoni et al., 2002)). αDG is a central member of the dystrophin glycoprotein complex family located in peripheral membranes, and proper αDG glycosylation is essential for it to bind to extracellular matrix proteins, such as laminin. FCMD patients manifest severe muscular dystrophy from early infancy along with intellectual disabilities, seizures, and insomnia because of a brain anomaly that occurs during the fetal period. They gradually become bedridden by their teenage years and need respiratory support and a feeding tube. They typically do not survive to their 20s and need lifelong systemic support from their families (Taniguchi-Ikeda et al., 2016).

FCMD is most frequently seen in Japan and other Asian countries. All FCMD patients in Japan possess the SINE-VNTR-*Alu* (SVA)-type retrotransposal insertion in at least one allele of the causative gene, *fukutin* (*FKTN*) (Kobayashi et al., 1998). We previously reported that FCMD is caused by a splicing anomaly induced by aberrant acceptor activity within the SVA insertion of the 3′-untranslated region (UTR) of *FKTN* (Taniguchi-Ikeda et al., 2011).

To date, we have studied FCMD using patient-derived primary myoblasts, lymphoblasts, and FCMD transgenic mouse models. However, FCMD mice do not fully recapitulate the phenotypes observed in human patients. A homozygous knock-in of humanized *fktn* with an SVA-type insertion does not show any muscular dystrophy symptoms or brain anomalies (Kanagawa et al., 2009); however, complete *fktn* knockout mice showed embryonic lethality (Kurahashi et al., 2005). In wild-type mice, *fktn* mRNA is detectable from embryonic day (E) 6.5 and is expressed in forebrain neuroepithelium on E9.5 (Horie et al., 2002). However,

[1]Department of Clinical Genetics, Fujita Health University Hospital, 1-98 Dengakugakubo, Kutsukake-chou, Toyoake, Aichi 470-1192, Japan

[2]Division of Molecular Genetics, Institute for Comprehensive Medical Science, Fujita Health University, Toyoake, Aichi 470-1192, Japan

[3]Department of Pediatrics, Kobe University Graduate School of Medicine, Kobe, Hyogo 650-0017, Japan

[4]Division of Advanced Medical Science, Graduate School of Science, Technology and Innovation, Kobe University, Kobe, Hyogo 650-0017, Japan

[5]Department of iPS Cell Applications, Graduate School of Medicine, Kobe University, Kobe, Hyogo 650-0017, Japan

[6]Center for Human Resource Development for Regenerative Medicine, Kobe University Hospital, Kobe, Hyogo 650-0017, Japan

[7]Department of Chemical Science and Engineering, Graduate School of Engineering, Kobe University, Kobe, Hyogo 657-8501, Japan

[8]Department of Clinical Application, Center for iPS Cell Research and Application, Kyoto University, Sakyo-ku, Kyoto 606-8507, Japan

[9]Department of Pediatrics, Kyoto University Graduate School of Medicine, Sakyo-ku, Kyoto 606-8507, Japan

[10]Department of Cellular Function Analysis, Research

Continued

fktn knockout mice are resorbed by E9.5 (Kurahashi et al., 2005), before the cerebral cortex fully forms neuronal circuits and architecture. This limits the ability of transgenic mice to reproduce FCMD brain anomalies.

FKTN has recently been identified as an *O*-mannosyl glycosyltransferase of ribitol-5 phosphate of αDG (Kanagawa et al., 2016). At least 18 enzymes thus far have been identified as being involved in the *O*-mannosylated glycosylation of αDG, and their deficiencies show similar phenotypes. They are thus collectively termed αDGpathies (Taniguchi-Ikeda et al., 2016). Deficient *O*-mannosylated glycosylation of αDG compromises its binding to laminin on the basement membrane. This abrogates its function, leading to structural fragility of the skeletal muscle membrane and dystrophic changes in muscle fibers (Taniguchi-Ikeda et al., 2016).

Other types of αDGpathies include dystroglycanopathy type A1 (MDDGA1, previously designated Walker-Warburg syndrome [WWS]) and muscle-eye-brain disease (MEB). MEB, which is mainly seen in European countries, is caused by homozygous or compound heterozygous mutations in the gene encoding protein *O*-mannosyltransferase-1 (POMT1; 607423). Dystroglycanopathy type A5; MDDGA5, which is caused by mutations in the gene encoding FKRP is also seen in European countries. Because these genes are responsible for *O*-mannose glycosylation, they share the same phenotypes, such as muscular dystrophy and brain anomaly, as FCMD. The common features in the CNS phenotype of α-dystroglycanopathies range widely from mild cognitive deficit to cobblestone lissencephaly and hydrocephalus. The phenotype severity is known to be correlated with the residual alpha dystroglycan glycosylation level in tissue (Mercuri et al., 2019).

In the central nervous system CNS, breaches in the glia limitans have been seen in FCMD fetal brains (Nakano et al., 1996), and studies based on mouse models have suggested a loss of radial glial (RG) guidance due to defects in αDG glycosylation (Nguyen et al., 2013). This, in turn, results in the disruption of proper neuronal migration in the developing brain, thus leading to brain anomalies (Myshrall et al., 2012; Nguyen et al., 2013; Sudo et al., 2018). Macroscopically, the surface of the cerebral cortex is cobblestone-like, or lissencephalic; and microscopically, the glia limitans showed frequent breaches at the surface of the brain at fetal week 18, suggesting disordered neuronal migration in the developing brain (Nakano et al., 1996). However, the mouse model commonly shows a milder phenotype in the CNS (Nickolls and Bonnemann, 2018). The discrepancy between the phenotype of the mouse model and human models is largely unknown. It would be extremely useful to be able to assess the initiation of and the point of no return in CNS abnormalities. However, fetal brain analyses of αDGpathies have been difficult due to limited sample availability, and mouse models cannot fully recapitulate the phenotype to reliably predict drug efficacy (Lui et al., 2011).

Thanks to extensive progress in cell culture technology, human pluripotent stem cells can now be differentiated into a brain-mimic neural identity in three-dimensional (3D) culture. *In vitro* 3D models of the human brain include the serum-free floating culture of embryoid body-like aggregates with quick reaggregation (SFEBq; (Eiraku et al., 2008)), cortical spheroids (Pasca et al., 2015), cerebral organoids (Lancaster et al., 2013), and forebrain organoids (Kadoshima et al., 2013). Brain organoids have enabled 3D architectural phenotypic analyses and are likely a better model to accurately study the neuronal network, predict clinical outcomes, and screen effective drugs for FCMD (Wang, 2018).

Basic research on gene therapies for muscular dystrophies, including αDGpathies, has progressed dramatically in recent years. In addition to gene therapies, low-molecular-weight compounds that may be able to treat intractable diseases, such as spinal muscular atrophy, have been successfully identified from a drug panel (Naryshkin et al., 2014). These compounds are low cost and can potentially cross the blood-brain barrier.

In this study, we employed the modified SFEBq method (Watanabe et al., 2017) that better mimics the laminar architecture of the developing cerebral cortex compared to other protocols (Kadoshima et al., 2013; Lancaster et al., 2013; Pasca et al., 2015). This is important to assess the architectural phenotypes seen in FCMD cerebral cortices. To recapitulate muscular dystrophy phenotypes of an FCMD patient, we used two additional model systems: induced pluripotent stem cell (iPSC)-derived myotubes and FCMD mouse models (Kanagawa et al., 2009).

Promotion and Support Headquarters, Fujita Health University, Toyoake, Aichi 470-1192, Japan

[11]Asubio Pharma Co., Ltd., Kobe, Hyogo 650-0047, Japan

[12]Innovative and Clinical Research Promotion Center, Gifu University Hospital, Yanagido, Gifu 501-1194, Japan

[13]Laboratory for Cell Asymmetry, RIKEN Center for Developmental Biology, Kobe, Hyogo 650-0047, Japan

[14]Department of iPS Cell Applied Medicine, Graduate School of Medicine, Kansai Medical University, Hirakata, Osaka 573-1010, Japan

[15]Department of Pediatrics, Tokyo Women's Medical University, School of Medicine, Shinjuku-ku, Tokyo 162-8666, Japan

[16]Department of Personalized Cancer Immunotherapy, Mie University Graduate School of Medicine, Tsu, Mie 514-8507, Japan

[17]Department of Neurobiology, David Geffen School of Medicine at the University of California, Los Angeles (UCLA), Los Angeles, CA 90095, USA

[18]Eli and Edythe Broad Center of Regenerative Medicine and Stem Cell Research, UCLA, Los Angeles, CA, USA

[19]Intellectual and Developmental Disabilities Research Center, UCLA, Los Angeles, CA 90095, USA

[20]Department of Neurology, Graduate School of Medicine, The University of Tokyo, Bunkyo-ku, Tokyo, 113-8655, Japan

[21]Department of Anatomy and Neurobiology, School of Medicine, University of California, Irvine, Irvine, CA 92697, USA

[22]Sue & Bill Gross Stem Cell Research Center, School of Medicine, University of California, Irvine, Irvine, CA 92697, USA

[23]Lead contact

*Correspondence: mtani@fujita-hu.ac.jp

https://doi.org/10.1016/j.isci.2021.103140

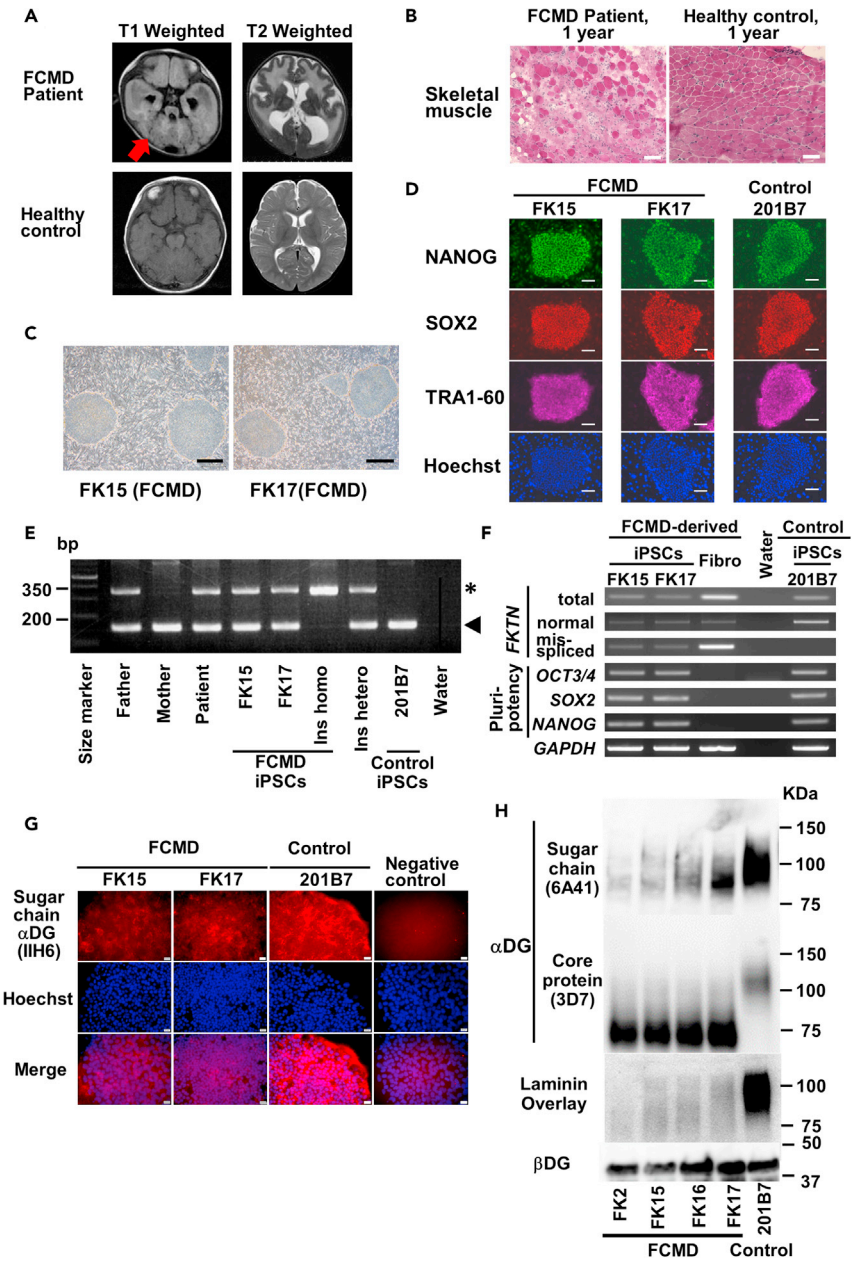

Figure 1. Alpha dystroglycan glycosylation is decreased in induced pluripotent stem cells derived from a Fukuyama congenital muscular dystrophy patient

(A) A transverse section of the patient's brain image. Magnetic resonance imaging showed severe lissencephaly and cerebellar cysts (arrow).

(B) Hematoxylin and eosin staining of the patient's skeletal muscle (biceps brachii) biopsy showed severe necrosis with abundant fibrotic tissue and partial fat replacement compared with an age-matched healthy control. Scale bar: 50 μm.

(C) Morphology of iPSC cells (FK15 and FK17) derived from a Fukuyama congenital muscular dystrophy (FCMD) patient. Scale bar: 500 μm.

(D) Characterization of pluripotency-marker expression in two induced pluripotent stem cell (iPSC) lines from the FCMD patient (FK15 and FK17) and a normal control (201B7) for NANOG (green), SOX2 (red), and TRA1-60 (magenta). Nuclei are counterstained with Hoechst (blue). Scale bars: 100 μm (white).

(E) Insertion PCR to detect the 3-kb-insertion–derived product (375 bp, upper band, asterisk) from patient iPSCs (FK15 and FK17), an FCMD patient homozygous for the insertion, and the genomic DNA of the FCMD patient and the parents extracted from peripheral blood. The normal *FKTN* gene is detected as the lower band (175 bp, arrow).

Figure 1. *Continued*

(F) Reverse-transcription PCR of *FTKN*, *OCT3/4*, *SOX2*, and *NANOG* expression in patient fibroblasts and iPSCs (FK15 and FK17) and a healthy control cell line (201B7). *GAPDH* was used as a loading control.

(G) Immunofluorescence analysis of patient iPSCs (FK15 and FK17) and control iPSCs (line: 201B7) for glycosylated alpha dystroglycan (αDG; clone: IIH6) and negative control for αDG staining. Scale bar: 20 μm.

(H) Western blotting of iPSCs for αDG glycans (clone: 6A41) and core protein (clone: 3D7) along with a laminin overlay assay. βDG: beta dystroglycan (loading control).

RESULTS

αDG glycosylation is decreased in iPSCs from an FCMD patient

FCMD patients with a deep-intronic mutation of *FKTN* intron 5 (c.647+2084G>T; p.Arg216SerfsTer10) in one allele and an SVA insertion in the other allele have a more severe phenotype than those with homozygous SVA insertions (Lim et al., 2010). To establish new FCMD disease models using human rather than animal cells, we generated iPSCs from an FCMD patient who possessed compound heterozygous variants in *FKTN*, i.e., a 3-kb SVA insertion (Figure S1A) and a deep-intronic variant at intron 5 (c.647+2084G>T; p.Arg216SerfsTer10; Figure S1B) (Kobayashi et al., 2017; Lim et al., 2010). The patient manifested severe muscular dystrophy, myopia, and brain anomalies. Brain magnetic resonance imaging showed severe lissencephaly and cerebellar cysts compared to age-matched healthy controls (Figure 1A). Histological analysis of a biceps brachii muscle biopsy showed necrotic muscle fibers and small regenerative muscle fibers with extensive fibrosis and fat replacement (Figure 1B). We established four FCMD-iPSC clones designated as FK2, FK15, FK16, and FK17 and validated by assessing their morphology, pluripotent marker expression, karyotype, and ability to differentiate into three germ layers. For a normal control, we employed the conventional iPSC line 201B7, which was first generated from a healthy donor by Yamakana's group (Takahashi et al., 2007). The FCMD iPSCs showed a human embryonic stem cell (hES)-like morphology (Figure 1C), expressed pluripotency markers (e.g., NANOG, SOX2, and TRA1-60; Figure 1D), had normal karyotypes (Figure S1C), and were able to differentiate into three germ layers *in vitro* (Figure S1D), similar to control iPSC line 201B7.

We then confirmed that the generated iPSCs had a 3-kb SVA insertion (Figures 1E and S1A) and a deep intronic pathogenic variant in intron 5 (Figures S1B and S1E), which was the same genotype as the patient donor (Figures S1A and S1B). Analyses of the *FKTN* transcripts also showed the expression of a 64-bp pseudoexon insertion between exons 5 and 6 caused by abnormal splicing in the patient-derived iPSCs but not normal control iPSCs (Figures 1F, S1B and S1F). Notably, normal *FKTN* was also expressed in patient-derived fibroblasts and iPSCs, although at a lower level than in the normal control (Figure 1F), which is consistent with previous findings in patient skeletal muscle (Taniguchi-Ikeda et al., 2011).

Next, we checked if the iPSCs recapitulated the reduced *O*-mannosyl glycosylation of αDG, which is the fundamental pathogenesis of FCMD. Antibody staining for αDG sugar chains (clone: IIH6) found decreased glycosylation in FCMD iPSCs compared to control iPSCs (Figure 1G). Western blotting also showed decreased αDG sugar chains (clone: 6A41) as well as a decreased molecular weight of the core αDG protein (clone: 3D7) compared to healthy control. In addition, decreased laminin binding was noted (Figure 1H), indicating impaired glycosylation of αDG in FCMD iPSCs.

The small-molecule compound Mannan-007 restored αDG glycosylation in FKTN-modified cell lines

We next evaluated the effect of the basic polycyclic compound Mannan-007 (Mn007), which has been reported to increase functional *O*-mannosyl glycans on αDG *in vitro* and *in vivo* by an unknown mechanism in myoblasts derived from patients with fukutin-related protein mutations, FCMD models, and healthy controls (Lv et al., 2015) Mn007 increased αDG glycosylation in human embryonic kidney cells (HEK 293 cells [HEK^{wt}]) in a dose-dependent manner (Figure 2A). Immunofluorescence showed that Mn007 increased staining of αDG sugar chains (clone: IIH6) and laminin (assessed by a laminin clustering assay), indicating glycan functionality (Figure 2B) (Kanagawa et al., 2009). To test if this effect was *FKTN*-dependent, we generated a *FKTN*-knockout HEK 293 cell line (HEK^{FKTN-}) using the CRISPR/Cas9 system (Figure S2, see STAR Methods). Mn007 did not increase αDG glycosylation in HEK^{FKTN-} cells (Figures 2A and 2C). In addition, the enhanced αDG glycosylation and its resulting increased molecular weight by Mn007 was restored when *FKTN* was re-expressed in HEK^{FKTN-} cells by transfecting them with a human *FKTN* cDNA construct ($FKTN^{wt}$; Figures 2C and S3A). Whereas the transfection of a mis-spliced *FKTN* cDNA construct

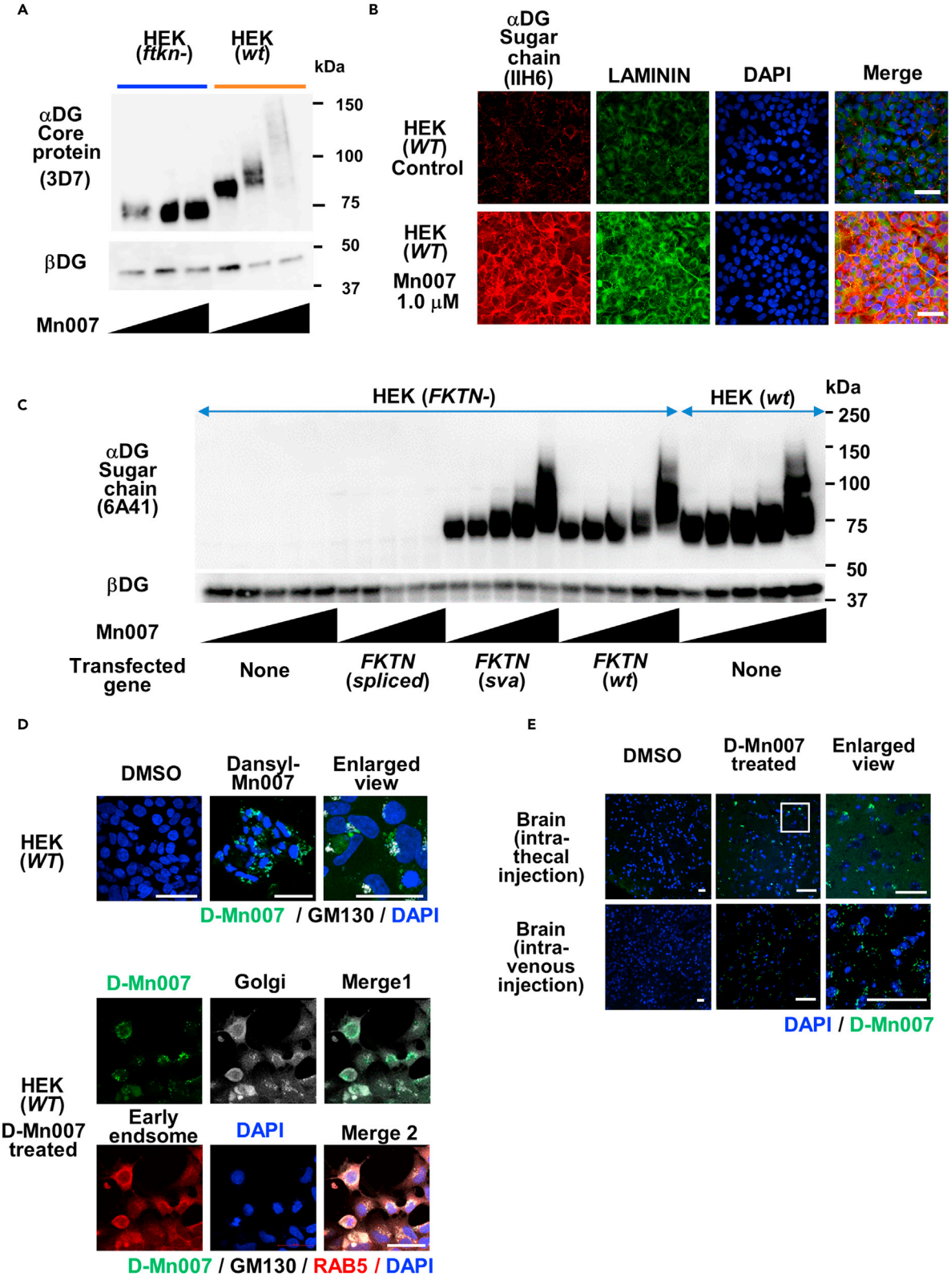
A
HEK (ftkn-)
HEK (wt)
kDa
αDG Core protein (3D7)
150
100
75
50
37
βDG
Mn007
B
αDG Sugar chain (IIH6)
LAMININ
DAPI
Merge
HEK (WT) Control
HEK (WT) Mn007 1.0 μM
C
HEK (FKTN-)
HEK (wt)
kDa
250
150
100
75
50
37
αDG Sugar chain (6A41)
βDG
Mn007
Transfected gene
None
FKTN (spliced)
FKTN (sva)
FKTN (wt)
None
D
DMSO
Dansyl-Mn007
Enlarged view
HEK (WT)
D-Mn007 / GM130 / DAPI
D-Mn007
Golgi
Merge1
HEK (WT) D-Mn007 treated
Early endsome
DAPI
Merge 2
D-Mn007 / GM130 / RAB5 / DAPI
E
DMSO
D-Mn007 treated
Enlarged view
Brain (intra-thecal injection)
Brain (intra-venous injection)
DAPI / D-Mn007

Figure 2. A small chemical compound increased alpha dystroglycan glycosylation in various Fukuyama congenital muscular dystrophy models
(A) Western blotting for alpha dystroglycan (αDG) core protein (clone: 3D7) in wild-type and *FKTN*-KO HEK cells treated with DMSO control (left) and 2 μM (middle) or 10 μM (right) Mannan-007 (Mn007). Beta-dystroglycan (βDG) was used as an internal loading control.
(B) Immunofluorescence of wild-type HEK cells treated with 1μM Mn007 or DMSO control (Control). The laminin clustering assay shows colocalization of cell-surface laminin with glycosylated αDG. Scale bar: 50 μm.
(C) Western blotting showing αDG glycosylation (clone: 6A41) in wild-type HEK cells; *FKTN*-knockout HEK cells; and *FKTN*-knockout HEK cells expressing a human patient *FKTN* cDNA sequence, a truncated mis-spliced *FKTN* gene, and human wild-type *FKTN*. Cells were treated with DMSO or Mn007 at a final concentration of 0, 0.2, 1, 2, or 10 μM. βDG was used as an internal loading control.
(D) Localization of dansyl-conjugated Mn007 (D-Mn007, green signal), the Golgi marker GM 130 (white, upper), and the early endosome marker Rab5 (red, lower) in HEK cells. Scale bar: 50 μm.
(E) Localization of D-Mn007 in brain tissue following intrathecal injection (middle) and intravenous injection (bottom). Scale bar: 50 μm.

(*FKTN*^{spliced}) that does not result in normal *FKTN* expression had no effect. The patient-type construct (*FKTN*^{sva}) that corresponds to a normal *FKTN*-coding sequence with a 3-kb SVA insertion in the 3′-UTR resulted in a dose-dependent increase in αDG glycosylation (Figures 2C and S3A), indicating that this chemical compound would be effective for FCMD patients with a slight amount of normal *FKTN* expression.

Next, we tested the intracellular localization and *in vivo* distribution of Mn007 with a fluorescent dansyl chloride-conjugated Mn007 (D-Mn007). Adding D-Mn007 to the medium of HEK cells resulted in fluorescence localization within the cytoplasm that partially overlapped with the ER and Golgi apparatus (Figure 2D). We then administered D-Mn007 intrathecally into the CNS. Two days after treatment, fluorescence signals were detected in the brain tissue of D-Mn007–treated mice but not in phosphate-buffered saline (PBS)–treated control mice (Control; Figure 2E). We also introduced D-Mn007 via the tail vein. We detected D-Mn007 signals in the brain within 24 h, suggesting that this chemical was able to pass the blood-brain barrier (Figure 2E).

Cortical organoids generated by SFEBq recapitulated the disordered neuronal migration of FCMD patients

To establish a human disease model of the CNS phenotype of FCMD that occurs during corticogenesis, the highly reproducible and efficient cerebral organoid differentiation method that was previously reported by Watanabe et al. was employed (Watanabe et al., 2017). FCMD patient-derived iPSCs (FK15 and FK17), control iPSCs (201B7), and control human embryonic stem cells (hESCs; KhES-1) were successfully differentiated into cerebral cortex. The median sizes (perimeter) of the FCMD patient organoids and healthy control organoids were 143.0 μm (interquartile range [IQR]: 133.1–152.8) and 152.3 μm (IQR: 138.0–164.5; $p = 0.041$), respectively, at 3 weeks and 210.7 μm (IQR: 184.9–225.9) and 241.8 μm (IQR: 210.4–260.7; $p < 0.001$) at 5 weeks (Figure 3A; Table S1). Immunofluorescence (IF) showed expression of FOXG1 (forebrain marker), PAX6 (dorsal cortical marker), and SOX2 (generic neural progenitor marker) in more than 80% of both FCMD and control organoids (Figure 3B).

We next observed cortical organoid architecture. A cobblestone-like, lumpy surface was present along the basal side of the FCMD organoids (Figures 3Ca, b [arrowheads], d and 3D) in contrast to the smooth surface seen in healthy control organoids (Figure 3Cf–i). The breached basal surface of these organoids (Figure 3Cb) more-closely resembled that of a fetal brain with FCMD at 16 weeks gestational age (Figure 3Ca, arrow) than age-matched control specimens (Figure 3Ce, permission to use the fetal picture was obtained from the Database of Histology Color Slides at Kobe Gakuin University). Radial glial cells stained radially with nestin from the rosette-like neuroepithelial layer (NEL) to the cortical plate layer and colocalized with αDG sugar chains (clone: IIH6, Figure 3Cf–h). However, staining for αDG sugar chains was absent in FCMD organoids (Figure 3Cc), and the staining pattern of radial glial cells was disorganized (Figure 3Cb). Despite this, laminin staining on the basal surface was not decreased in FCMD organoids compared to control organoids (Figure 3Cd, i). RG cell expression of nestin in FCMD organoids showed a disorganized architecture in both the radial and parietal directions (Figure 3Cb). In addition, we observed many breaches extruded from the surface of FCMD organoids (Figures 3Cb, 3D [arrowheads on FK15 and FK17]) in contrast to the smooth surface seen in the control organoids (Figure 3D, arrows on 201B7 and KhES-1), suggesting the overmigration of radial fibers and neurons. Quantifying the ratio of breaches in each organoid NEL showed significantly higher ratios in FCMD organoids (72%) than in control organoids (8%; Figure 3D and Table S2).

We further analyzed the cortical layer architecture, neuronal migration, and RG cells of FCMD organoids. Rosette-like neuroepithelial layers were seen in both FCMD organoids and healthy controls from 5 to

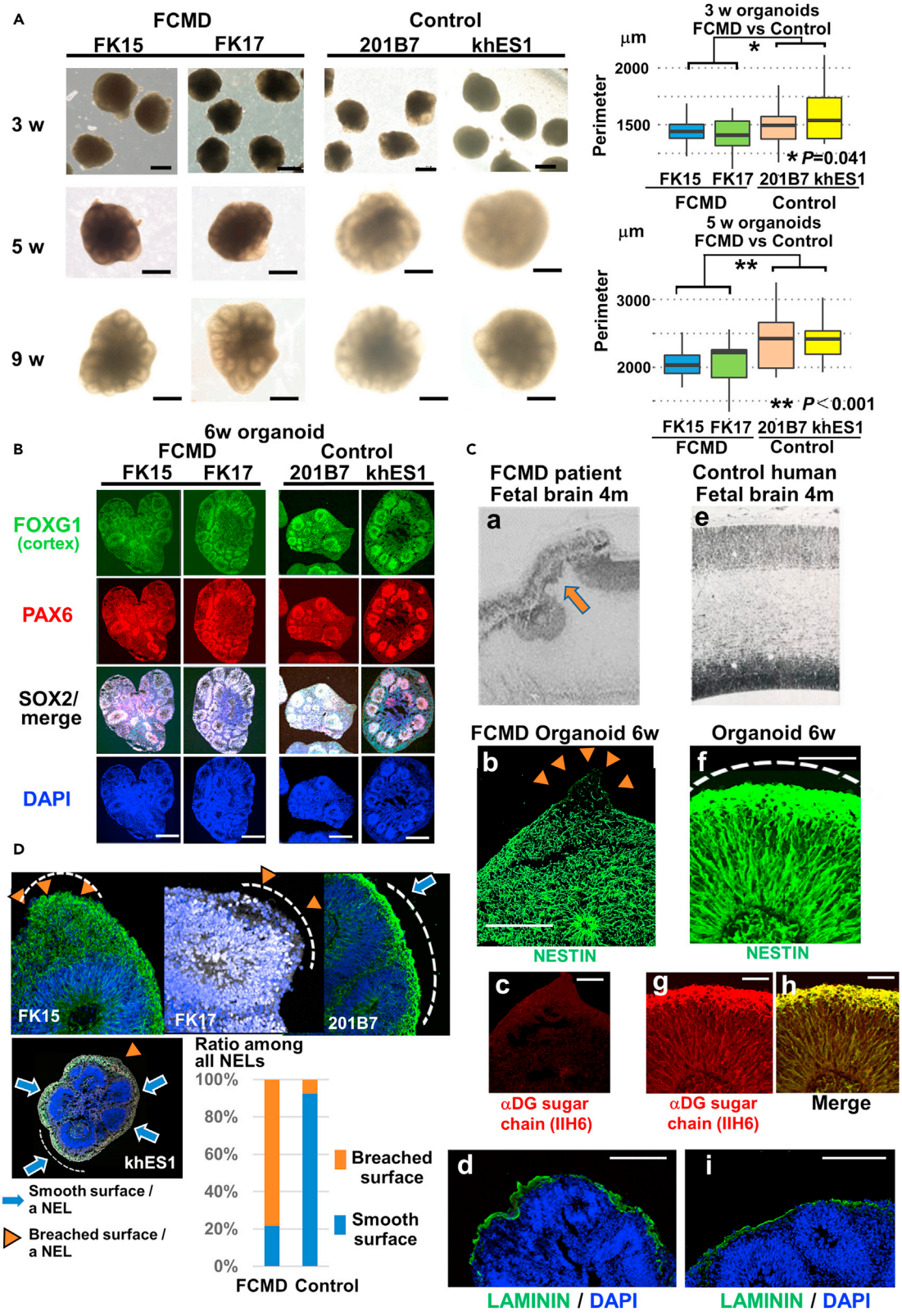
A
FCMD
FK15
FK17
Control
201B7
khES1
3 w
5 w
9 w
3 w organoids
FCMD vs Control
μm
Perimeter
2000
1500
*
* P=0.041
FK15 FK17 201B7 khES1
FCMD
Control
5 w organoids
FCMD vs Control
3000
2000
**
** P<0.001
B
6w organoid
FOXG1
(cortex)
PAX6
SOX2/
merge
DAPI
C
FCMD patient
Fetal brain 4m
Control human
Fetal brain 4m
a
e
FCMD Organoid 6w
Organoid 6w
b
f
NESTIN
NESTIN
c
g
h
αDG sugar
chain (IIH6)
αDG sugar
chain (IIH6)
Merge
D
FK15
FK17
201B7
khES1
Smooth surface /
a NEL
Breached surface /
a NEL
Ratio among
all NELs
100%
80%
60%
40%
20%
0%
Breached
surface
Smooth
surface
FCMD Control
d
i
LAMININ / DAPI
LAMININ / DAPI

Figure 3. 3D brain organoids derived from induced pluripotent stem cells derived from a Fukuyama congenital muscular dystrophy patient

(A) Representative brightfield images of organoids generated by serum-free cultures of embryoid body-like aggregates with quick reaggregation (SFEBq) after 3, 5, and 9 weeks of aggregation. Organoids derived from induced pluripotent stem cells (iPSCs) from a patient with Fukuyama congenital muscular dystrophy (FCMD; FK15 and FK17), control iPSCs (201B7) and control human embryonic stem cells (KhES-1). Scale bar: 500 μm. We analyzed the size of organoids (n = 20) derived from 2 FCMD and 2 control iPSC lines at 3 and 5 weeks (each clone from 10 SFEBq independent experiments, bar indicates median perimeter). We didn't analyze the size for 9-week old organoids since organoids were cut after 5 weeks. The data were analyzed by the Mann-Whitney U test. *$p < 0.001$.

(B) Representative immunofluorescence (IF) staining of 6-week–organoid sections for FOXG1 (cortex marker, green), PAX6 (neural progenitor, red), and SOX2 (neural progenitor, white), along with DAPI nuclear counterstaining. Scale bar: 200 μm.

(C) (a) Nissl-stained fetal cerebral cortex section from an FCMD patient (gestational age: 16 weeks). (b–d) Representative IF staining of a 6-week FCMD organoid for: (b) nestin (green) showing the neuroepithelial layer (NEL) and radial glia (RG), (c) sugar chain of alpha dystroglycan (αDG, clone: IIH6, red), laminin (green), and DAPI (blue). (e) A Nissl-stained 16-weeks gestational age control fetal cerebral cortex section. Normal control 6-week organoid stained for: (f) nestin (green) showing the RGs of the ventricular zone (VZ) to the cortical plate (CP), (g) sugar chain of αDG (clone: IIH6, red), (h) colocalization of nestin with the αDG sugar chain, and (i) laminin (green), and DAPI (blue). The dotted line in (f) outlines the smooth surface of the organoid. Scale bar: 100 μm.

(D) Quantification of the ratio of breached NEL on the organoids' basal surface as a proportion of the entire NEL. Organoids were stained with nestin (green), SOX2 (white), and DAPI (blue). Orange arrowheads and the dotted line indicate breached NELs, whereas the blue arrows and dotted line indicate a smooth NEL surface ($n = 20$ replicates of each clone, the data were analyzed by Fisher's exact test, $p < 0.001$).

12 weeks (Figures 3A, 3B, 4A and S4A). We observed deeper-layer neuronal markers, such as TBR1 and CTIP2, in the cortical plate-like region above the ventricular zone at 7 weeks (Figure 4A) in both FCMD and control organoids. In control organoids, the ventricular zones stained densely for SOX2, the cortical plates stained for both TBR1 and CTIP2, and subventricular zones were between these layers (Figure 4A, lower panels). These layers could be easily distinguished in control organoids. However, FCMD organoids did not have distinct layers that were easily recognized. We measured the distance from the basal edge of the ventricular zone to the basal edge of the cortical layer. The box plot shows that the width of FCMD organoids (median: 125.0 μm, IQR: 78.8–158.8 μm) was significantly greater in comparison to that of normal control organoids (median: 60 μm, IQR: 41.9–75.0 μm; $P < 0.001$, Figure 4B and Table S3). The distributions of TBR1-positive cells and CTIP2-positive cells above the margin of the FCMD organoid VZ were significantly more scattered than the normal control organoid (Figure 4C, $p < 0.001$, and Table S4). Apoptotic marker and proliferation marker such as caspase-3 and Ki67, respectively, were not increased (data not shown).

Next, we labeled glial progenitors by introducing GFP-expressing plasmids driven by a PGK promoter (EF-PGK-GFP) into the apical side of FCMD and control organoids to visualize RG fiber migration. GFP expression was successfully induced 24 h after electroporation of EF-PGK-GFP. At 48 h after transfection, the GFP-expressing cells showed a bipolar shape (Figure 4D, left 2 columns), suggesting a glial morphology. These GFP-positive RG fiber migrated upward and reached the basal surface of the organoid surface, subsequently breaching along with CTIP2-positive neurons (Figure 4D, enlarged view, white arrows). Nestin and p-vimentin staining were scattered in FCMD organoids compared to the radially and parietally organized staining patterns seen in healthy controls (Figure S4B).

Mn007 partially restored glycosylation in FCMD iPSCs and their derivatives: myotubes and brain organoids

Western blotting of iPSC lines showed a distinct increase in αDG glycosylation after treatment with 1 μM Mn007 (Figure S3B). The effects of Mn007 on the myotubes generated from FCMD- and healthy iPSCs by overexpressing the *MYOD* gene was also tested (Tanaka et al., 2013). Although the size and shape of the myotube fibers were not markedly different between those derived from FCMD- and healthy iPSCs, FCMD-derived myotubes showed reduced staining for glycosylated αDG as well as a decreased laminin clustering, which suggested a decrease in the amount of functional αDG in these myotubes (Figure 5A). Mn007 treatment increased colocalization of glycosylated αDG with laminin and restored laminin clustering, suggesting an increase in functional αDG (Figure 5B).

To evaluate the effect in cortical organoid models, organoids were treated with Mn-007. Brain organoids treated with 1 μM Mn007 for 2 weeks also showed increased staining for the sugar chain of αDG (clone: IIH6) in 10-week cerebral cortices (Figure 5C). Mn007 induced growth arrest at concentrations over 2 μM, but long-term 1 μM treatment did not induce any toxicity in our system. The laminin staining pattern was unaltered (data not shown). In treated organoids, the layered distribution of TBR1 and CTIP2 was partially rescued (Figure 5D).

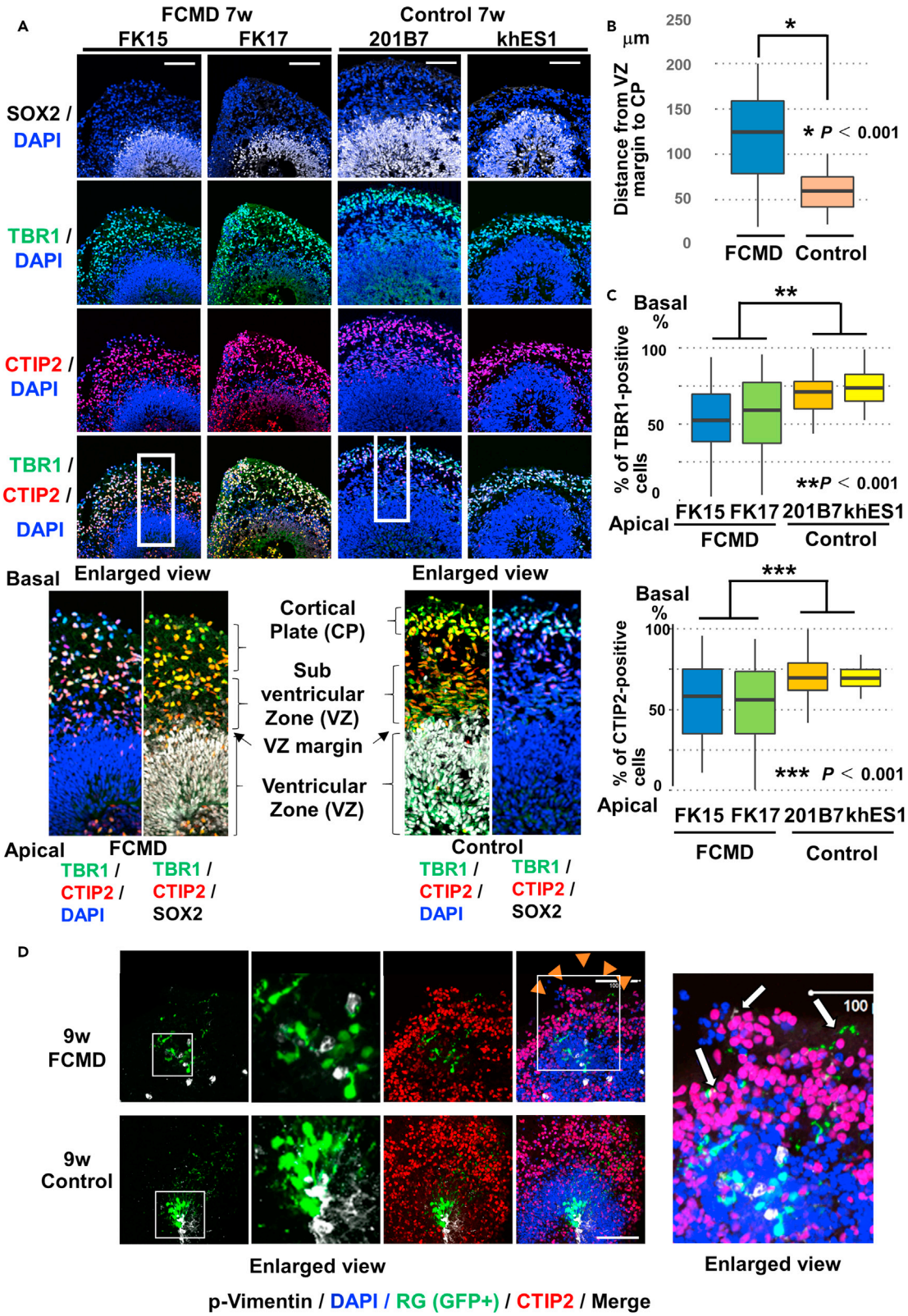
A
FCMD 7w
Control 7w
FK15
FK17
201B7
khES1
SOX2 / DAPI
TBR1 / DAPI
CTIP2 / DAPI
TBR1 / CTIP2 / DAPI
Basal
Enlarged view
Enlarged view
Cortical Plate (CP)
Sub ventricular Zone (VZ)
VZ margin
Ventricular Zone (VZ)
Apical
FCMD
Control
TBR1 / CTIP2 / DAPI
TBR1 / CTIP2 / SOX2
B
μm
Distance from VZ margin to CP
250
200
150
100
50
0
* P < 0.001
FCMD
Control
C
Basal
%
% of TBR1-positive cells
100
50
0
** P < 0.001
Apical
FK15 FK17 201B7 khES1
FCMD
Control
***
% of CTIP2-positive cells
*** P < 0.001
D
9w FCMD
9w Control
100
Enlarged view
Enlarged view
p-Vimentin / DAPI / RG (GFP+) / CTIP2 / Merge

Figure 4. 3D Fukuyama congenital muscular dystrophy brain organoids showed a disorganized radial glial orientation

(A) Immunofluorescence analysis of 7-week Fukuyama congenital muscular dystrophy (FCMD) and control organoids (201B7 and KhES-1) for deep neuronal layer markers, TBR1 (green) and CTIP2 (red), and neuronal progenitors, SOX2 (white). Scale bar: 100 μm.

(B) Measurement of the width of the cortical plate (CP)-like region above the ventricular zone (VZ). Box plot comparing the median of the maximum lengths of 20 neuroepithelial layers from 7-week FCMD and control organoids. The data were analyzed by the Mann–Whitney U test ($p < 0.001$).

(C) Measurement of the distribution of CTIP2- and TBR1-positive neurons in the cortical layers of IHC organoid sections. The distributions of each positive cell were measured as the percentile, as the % distance of the cells above the margin of the VZ to the surface of the organoids. The box plot indicates the upper extreme (top bar), upper quartile (top of the box), median (bar), mean (x), lower quartile (bottom of the box), and lower extreme (bottom bar), with these values listed in Table S3. The Mann–Whitney U test was used to analyze group differences in distribution. Asterisks indicate $p < 0.001$.

(D) Migration of radial glial fibers (RGs) in organoids. Organoid sections 48 h after electroporation of the GFP-expression plasmid into RGs showing GFP-positive RGs (green), p-vimentin (white), CTIP2 (red), and DAPI (blue). Arrowhead: extruded neurons, arrows: overmigrated RG fibers. Scale bar: 100 μm.

Administration of rhodamine-conjugated Mn007 to brain organoids for 48h resulted in its localization around nuclei of a wide range of NELs (Figure 5E). In summary, Mn007 restored a healthy phenotype in our patient iPSC-derived disease models.

DISCUSSION

This study is the first to establish a fetal human brain model of FCMD, a type of αDGpathy, using 3D brain organoids generated from FCMD-patient-derived iPSCs. In this decade, the function of αDG in the development and maintenance of brain neural networks has been investigated (Nickolls and Bonnemann, 2018). Cell type-specific deletion of αDG in mice revealed that glial but not neuronal dystroglycan is involved in forebrain development (Satz et al., 2010). On the other hand, defects in dystroglycan glycosylation caused by mutation of Large, a glycosyltransferase necessary for the normal glycosylation of dystroglycan, resulted in lissencephaly in mice (Michele et al., 2002), and heavily glycosylated αDG was continuously localized on the normal pial basement membrane (Myshrall et al., 2012), suggesting the importance of αDG glycosylation in corticogenesis. Furthermore, mouse models suggested that radial glia anchored to the pial basement membrane act as a guiding scaffold (Nickolls and Bonnemann, 2018); and a discontinuous pial basement membrane—a finding seen in the brain of human fetuses with FCMD (Nakano et al., 1996) —was reportedly observed in various mouse models of alpha dystroglycanopathy, such as myodystrophy mice, albeit to a lesser extent (Michele et al., 2002). Taken together, deficits in alphaDG glycosylation would lead to disorganized radial glial endfeet, which would—in turn—lead to the abnormal migration of neuronal cells. Based on this hypothesis, mice with mutant FKTN, a glycosyltransferase of αDG, had been expected to recapitulate brain abnormality in FCMD. However, an FCMD mouse model generated by knocking in the 3-kb FKTN SVA did not show any brain anomalies (Kanagawa et al., 2009), and a dorsal telencephalon-specific conditional *fktn* knockout mice showed only slight discontinuity of the pial basement membrane but not laminar disorganization of the cortex (Sudo et al., 2018). The size and surface area of the human neocortex are substantially different from the rodent neocortex, partially due to the massive expansion of the SVZ and outer RG formation, which would lead to increased neuron numbers and networks in the human brain in comparison to the rodent brain (Heide et al., 2018; Lui et al., 2011). These developmental distinctions and possible differential DG requirements among distinct species would explain why murine models cannot recapitulate the brain abnormalities of FCMD.

Using our SFEBq differentiation system, we demonstrated that our brain organoids were able to generate distinct laminar organization and anatomical changes in FCMD organoids relative to healthy controls, which have not been recapitulated in FCMD mouse models. This model allowed us to test the RG fiber migration and neuronal distribution in organoids, recapitulating human corticogenesis and the abnormal fiber organization seen in FCMD patients. Although we were not able to properly induce glia limitans or pia mater formation, in which the rupturing of neuronal migration is observed in the FCMD fetal brain, we did mimic neuron over-migration, which was likely misguided by disorganized RG fibers. *O*-mannosyl–glycosylated αDG colocalized with nestin in healthy control organoids, generating a radially and parietally organized apicobasal structure that mimicked the developing fetal brain; this suggests that RG fibers can be properly guided by *O*-mannosyl glycans. Probably due to the lack of αDG sugar chains in FCMD organoids, the nestin staining and surface architecture became quite disorganized, with neurons migrating in scattered directions, and the migration distance seeming uncontrolled. These data support the hypothesis that deficits of glycosylation in glial αDG—not neuronal αDG—may be the cause of this over-migration and the breached brain surface seen in patient brain pathology.

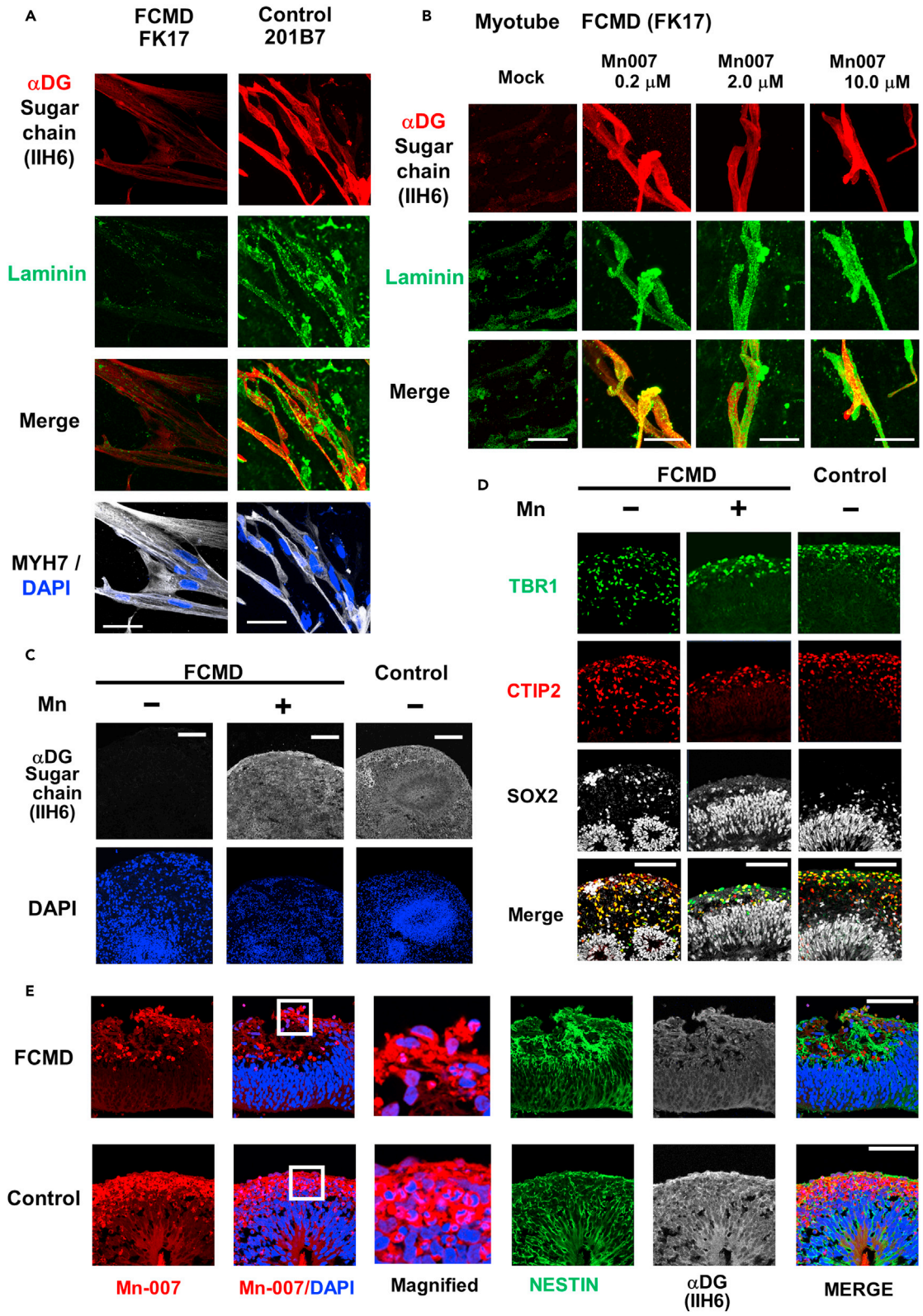
A
FCMD FK17
Control 201B7
αDG Sugar chain (IIH6)
Laminin
Merge
MYH7 / DAPI
B
Myotube
FCMD (FK17)
Mock
Mn007 0.2 μM
Mn007 2.0 μM
Mn007 10.0 μM
αDG Sugar chain (IIH6)
Laminin
Merge
C
FCMD
Control
Mn
αDG Sugar chain (IIH6)
DAPI
D
FCMD
Control
Mn
TBR1
CTIP2
SOX2
Merge
E
FCMD
Control
Mn-007
Mn-007/DAPI
Magnified
NESTIN
αDG (IIH6)
MERGE

Figure 5. The small chemical compound Mannan-007 increased alpha dystroglycan glycosylation in iPSC-derived Fukuyama congenital muscular dystrophy models

(A) Myotubes derived from induced pluripotent stem cells (iPSCs) from a patient with Fukuyama congenital muscular dystrophy (FCMD; FK17) and a healthy control (201B7) were stained for the sugar chain of alpha dystroglycan (αDG, clone: IIH6, red), laminin (green), the skeletal muscle marker myosin heavy chain 7 (MYH7, white), and DAPI counterstain (blue). Scale bar: 50 μm.

(B) Myotubes derived from FCMD iPSCs showing αDG glycosylation (clone: IIH6, red) and laminin clustering (green) after treatment with DMSO control or 1, 2, and 10 μM Mannan-007 (Mn007).

(C) Staining for αDG glycosylation (clone: IIH6, white) in brain organoids treated with Mn007 (Mn).

(D) The migration of TBR1 (green)-positive neurons and CTIP2 (red)-positive neurons in 10-week FCMD organoids after Mn007 treatment compared to untreated control organoids and 10-week healthy control organoids.

(E) Rhodamine-conjugated Mn007 (red) localized around the nuclei of neuroepithelial layer cells (Magnified view) within 10-week organoids (FCMD and control) 48 h after rhodamine-Mn007 (2 μM) was applied to the medium (upper, FCMD; lower, healthy control). Organoids were stained for nestin (green), the sugar chain of αDG, clone IIH6 (white), and counterstained with DAPI (blue). Scale bar: 100 μm.

We also restored functional αDG in various models, particularly in the CNS, with the basic polycyclic compound Mn007 and corrected the abnormal neuronal migration seen in patient organoids. Since the FCMD mouse model lacks the phenotype in CNS tissue, we first showed that the chemical was effective in restoring the CNS architecture using a 3D cortical organoid model. The compound was FKTN-dependent and successfully restored αDG sugar chains in cells expressing an FCMD variant FKTN cDNA as well as in the FCMD mouse model. Mn007 increased the laminin binding of αDG, suggesting that glycosylated αDG is still functional. These findings suggest that Mn007 might be a viable therapeutic option for FCMD patients in the future. We first need to clarify the mechanism underlying the enhancement of αDG glycosylation that is induced by this chemical compound, as well as its possible toxicity.

The detection of D-Mn007 in brain tissue following its intravenous injection indicates that this chemical compound can cross the blood-brain barrier. It may therefore be a viable prenatal treatment for migration disorder that may also lead to systemic αDG recovery in FCMD patients. In 10-week-old FCMD organoids, which correspond to the approximately 14-week-old fetal brain, when the neurons migrate rapidly to form cortical layers, 2 weeks of Mn007 treatment restored glycosylated αDG and partially recovered the normal architecture (Watanabe et al., 2017). The restored orientation of RG fiber migration may constitute a radical treatment for the CNS symptoms of FCMD patients. We have not tested whether or not this chemical can cross the blood-placental barrier; however, if so, it may be an option for treating the migration disorder seen in FCMD fetuses.

This organoid model recapitulated the phenotype of human FCMD, and a small chemical compound corrected αDG glycosylation in various FCMD models, restoring the function of αDG and correcting neuron migration. These results could be used to further clarify the molecular mechanisms underlying the migration defects caused by deficient αDG O-mannosyl glycosylation in FCMD.

Limitations of the study

Although our studies show that the application of Mn007 could partially rescue cortical neurogenesis brain organoids derived from FCMD patient iPSC, the mechanism(s) of its actions remain unclear. A better understanding of how it interacts with glycans could help in the development of more potent analogues or perhaps identify additional therapeutic targets that act through same or complementary pathways. Though Mn007 had encouraging effects in our brain organoid model, further testing will be needed to confirm its efficacy in ameliorating skeletal muscle and brain developmental defects *in vivo*. In addition, given that FCMD impacts corticogenesis at such an early stage of development, further studies are needed to define the optimal time at which Mn007 would need to be administered to achieve maximal therapeutic benefit.

STAR★METHODS

Detailed methods are provided in the online version of this paper and include the following:

- KEY RESOURCES TABLE
- RESOURCE AVAILABILITY
  - Lead contact
  - Material availability

SUPPLEMENTAL INFORMATION

Supplemental information can be found online at https://doi.org/10.1016/j.isci.2021.103140.

ACKNOWLEDGMENTS

We would like to thank Kana Sugahara, S.N., Tomoko Yashiro, Aya Kubota, Michiko Ujihara, Ayaka Nishiyama, Ryou Yoshida, Yuko Takeuchi, Rena Takeda, Tatsuro Ikeda, Aasami Kita, Yu Furuno, Akiko Kojima, Katsuyuki Yokoi, Khaledian Behnoush and Takema Kato for technical support. We would like to thank Drs. Hiroshi Manya, Keiichiro Inamori, and Akitsu Hotta, Professors Fumio Matsuzaki, Ichiro Morioka, Yoshiki Yamaguchi, Kazumoto Iijima, Tamao Endo, and Naoyuki Taniguchi for their valuable comments. We would like to thank Drs. Helena A. Popiel and Allison C. Sharrow for editing and proof-reading the manuscript. This research was supported by grants from the Japan Agency for Medical Research and Development (17ek0109193h0002 to MTI, TA, and KM; 20ek0109318h0003 to MTI, MKA, TM, and TA; 20ek0109405h0002 to HS, and MTI; 18ek0109249h0002 to TT, MTI, and KI, 21bm0804028h0001 to MTI, MKA), Grants-in-Aid for Scientific Research (18K07790 to MTI and IK, 21H02885 to MTI, TA, MKA, TM, and KI), The Naito Foundation (to MTI), Japan Intractable Disease Foundation (to MTI), Takeda Science Foundation (to MTI), Houansya Foundation (to MTI), Akira Sakagami Fund for Research and Education from Kobe University Graduate School of Medicine (to TA), and Research Assistance Funds from the General Incorporated Association Shinryokukai (to TA), National Institute of Health (R01NS089817, R01DA051897, and P50HD103557 to BGN; K99/R00HD096105 to MW), the California Institute for Regenerative Medicine (DISC1-08819 to BGN), and the UCLA Broad Stem Cell Research Center (BSCRC) to BGN, and training awards provided by the UCLA BSCRC, UCLA Brain Research Institute, and the Uehara Memorial Foundation to MW.

AUTHOR CONTRIBUTIONS

Conceptualization: MTI, TA; Methodology: MTI, TA, MKA TM HS SN, TT HT TK; Validation: MKA, HS, TT, HT; Investigation: MTI, MKA, AH, TA; Visualization: MTI, AH, AM, KI; Statistical Analysis: T.I; Resources: AM, KI; Funding acquisition: MTI, TA, TT; Project administration: MTI, TA; Supervision: MW, BGN, KM, TT; Writing – original draft: MTI, TA, MW, MKA, and TM; Writing – review & editing: MTI, TA, MKA, and MW.

DECLARATION OF INTERESTS

The authors declare that the research was conducted in the absence of any commercial or financial relationships that could be construed as a potential conflict of interest.

Received: April 26, 2021
Revised: August 11, 2021
Accepted: September 14, 2021
Published: October 22, 2021

REFERENCES

Eiraku, M., Watanabe, K., Matsuo-Takasaki, M., Kawada, M., Yonemura, S., Matsumura, M., Wataya, T., Nishiyama, A., Muguruma, K., and Sasai, Y. (2008). Self-organized formation of polarized cortical tissues from ESCs and its active manipulation by extrinsic signals. Cell Stem Cell *3*, 519–532. https://doi.org/10.1016/j.stem.2008.09.002.

Fukuyama, Y., Osawa, M., and Suzuki, H. (1981). Congenital progressive muscular dystrophy of the Fukuyama type - clinical, genetic and pathological considerations. Brain Dev. *3*, 1–29. https://doi.org/10.1016/s0387-7604(81)80002-2.

Heide, M., Huttner, W.B., and Mora-Bermudez, F. (2018). Brain organoids as models to study human neocortex development and evolution. Curr. Opin. Cel. Biol. *55*, 8–16. https://doi.org/10.1016/j.ceb.2018.06.006.

Horie, M., Kobayashi, K., Takeda, S., Nakamura, Y., Lyons, G.E., and Toda, T. (2002). Isolation and characterization of the mouse ortholog of the Fukuyama-type congenital muscular dystrophy gene. Genomics *80*, 482–486.

Kadoshima, T., Sakaguchi, H., Nakano, T., Soen, M., Ando, S., Eiraku, M., and Sasai, Y. (2013). Self-organization of axial polarity, inside-out layer pattern, and species-specific progenitor dynamics in human ES cell-derived neocortex. Proc. Natl. Acad. Sci. U. S. A. *110*, 20284–20289. https://doi.org/10.1073/pnas.1315710110.

Kanagawa, M., Kobayashi, K., Tajiri, M., Manya, H., Kuga, A., Yamaguchi, Y., Akasaka-Manya, K., Furukawa, J.I., Mizuno, M., Kawakami, H., et al. (2016). Identification of a post-translational modification with ribitol-phosphate and its defect in muscular dystrophy. Cell Rep. *14*, 2209–2223. https://doi.org/10.1016/j.celrep.2016.02.017.

Kanagawa, M., Nishimoto, A., Chiyonobu, T., Takeda, S., Miyagoe-Suzuki, Y., Wang, F., Fujikake, N., Taniguchi, M., Lu, Z., Tachikawa, M., et al. (2009). Residual laminin-binding activity and enhanced dystroglycan glycosylation by LARGE in novel model mice to dystroglycanopathy. Hum. Mol. Genet. *18*, 621–631. https://doi.org/10.1093/hmg/ddn387.

Kim, D., Kim, C.H., Moon, J.I., Chung, Y.G., Chang, M.Y., Han, B.S., Ko, S., Yang, E., Cha, K.Y., Lanza, R., and Kim, K.S. (2009). Generation of human induced pluripotent stem cells by direct delivery of reprogramming proteins. Cell Stem Cell *4*, 472–476. https://doi.org/10.1016/j.stem.2009.05.005.

Kobayashi, K., Kato, R., Kondo-Iida, E., Taniguchi-Ikeda, M., Osawa, M., Saito, K., and Toda, T. (2017). Deep-intronic variant of fukutin is the most prevalent point mutation of Fukuyama congenital muscular dystrophy in Japan. J. Hum. Genet. *62*, 945–948. https://doi.org/10.1038/jhg.2017.71.

Kobayashi, K., Nakahori, Y., Miyake, M., Matsumura, K., Kondo-Iida, E., Nomura, Y., Segawa, M., Yoshioka, M., Saito, K., Osawa, M., et al. (1998). An ancient retrotransposal insertion causes Fukuyama-type congenital muscular dystrophy. Nature *394*, 388–392. https://doi.org/10.1038/28653.

Kurahashi, H., Taniguchi, M., Meno, C., Taniguchi, Y., Takeda, S., Horie, M., Otani, H., and Toda, T. (2005). Basement membrane fragility underlies embryonic lethality in fukutin-null mice. Neurobiol. Dis. *19*, 208–217. https://doi.org/10.1016/j.nbd.2004.12.018.

Lancaster, M.A., Renner, M., Martin, C.A., Wenzel, D., Bicknell, L.S., Hurles, M.E., Homfray, T., Penninger, J.M., Jackson, A.P., and Knoblich, J.A. (2013). Cerebral organoids model human brain development and microcephaly. Nature *501*, 373–379. https://doi.org/10.1038/nature12517.

Lim, B.C., Ki, C.S., Kim, J.W., Cho, A., Kim, M.J., Hwang, H., Kim, K.J., Hwang, Y.S., Park, W.Y., Lim, Y.J., et al. (2010). Fukutin mutations in congenital muscular dystrophies with defective glycosylation of dystroglycan in Korea. Neuromuscul. Disord. *20*, 524–530. https://doi.org/10.1016/j.nmd.2010.06.005.

Lui, J.H., Hansen, D.V., and Kriegstein, A.R. (2011). Development and evolution of the human neocortex. Cell *146*, 18–36. https://doi.org/10.1016/j.cell.2011.06.030.

Lv, F., Li, Z.F., Hu, W., and Wu, X. (2015). Small molecules enhance functional O-mannosylation of Alpha-dystroglycan. Bioorg. Med. Chem. *23*, 7661–7670. https://doi.org/10.1016/j.bmc.2015.11.011.

Mercuri, E., Bonnemann, C.G., and Muntoni, F. (2019). Muscular dystrophies. Lancet *394*, 2025–2038. https://doi.org/10.1016/S0140-6736(19)32910-1.

Michele, D.E., Barresi, R., Kanagawa, M., Saito, F., Cohn, R.D., Satz, J.S., Dollar, J., Nishino, I., Kelley, R.I., Somer, H., et al. (2002). Post-translational disruption of dystroglycan-ligand interactions in congenital muscular dystrophies. Nature *418*, 417–422. https://doi.org/10.1038/nature00837.

Muntoni, F., Brockington, M., Blake, D.J., Torelli, S., and Brown, S.C. (2002). Defective glycosylation in muscular dystrophy. Lancet *360*, 1419–1421. https://doi.org/10.1016/S0140-6736(02)11397-3.

Myshrall, T.D., Moore, S.A., Ostendorf, A.P., Satz, J.S., Kowalczyk, T., Nguyen, H., Daza, R.A., Lau, C., Campbell, K.P., and Hevner, R.F. (2012). Dystroglycan on radial glia end feet is required for pial basement membrane integrity and columnar organization of the developing cerebral cortex. J. Neuropathol. Exp. Neurol. *71*, 1047–1063. https://doi.org/10.1097/NEN.0b013e318274a128.

Nakano, I., Funahashi, M., Takada, K., and Toda, T. (1996). Are breaches in the glia limitans the primary cause of the micropolygyria in Fukuyama-type congenital muscular dystrophy (FCMD)? Pathological study of the cerebral cortex of an FCMD fetus. Acta Neuropathol. *91*, 313–321. https://doi.org/10.1007/s004010050431.

Naryshkin, N.A., Weetall, M., Dakka, A., Narasimhan, J., Zhao, X., Feng, Z., Ling, K.K., Karp, G.M., Qi, H., Woll, M.G., et al. (2014). Motor neuron disease. SMN2 splicing modifiers improve motor function and longevity in mice with spinal muscular atrophy. Science *345*, 688–693. https://doi.org/10.1126/science.1250127.

Nguyen, H., Ostendorf, A.P., Satz, J.S., Westra, S., Ross-Barta, S.E., Campbell, K.P., and Moore, S.A. (2013). Glial scaffold required for cerebellar granule cell migration is dependent on dystroglycan function as a receptor for basement membrane proteins. Acta Neuropathol. Commun. *1*, 58. https://doi.org/10.1186/2051-5960-1-58.

Nickolls, A.R., and Bonnemann, C.G. (2018). The roles of dystroglycan in the nervous system: insights from animal models of muscular dystrophy. Dis. Model Mech. *11*, dmm035931. https://doi.org/10.1242/dmm.035931.

Okita, K., Matsumura, Y., Sato, Y., Okada, A., Morizane, A., Okamoto, S., Hong, H., Nakagawa, M., Tanabe, K., Tezuka, K., et al. (2011). A more efficient method to generate integration-free human iPS cells. Nat. Methods *8*, 409–412. https://doi.org/10.1038/nmeth.1591.

Pasca, A.M., Sloan, S.A., Clarke, L.E., Tian, Y., Makinson, C.D., Huber, N., Kim, C.H., Park, J.Y., O'Rourke, N.A., Nguyen, K.D., et al. (2015). Functional cortical neurons and astrocytes from human pluripotent stem cells in 3D culture. Nat. Methods *12*, 671–678. https://doi.org/10.1038/nmeth.3415.

Satz, J.S., Ostendorf, A.P., Hou, S., Turner, A., Kusano, H., Lee, J.C., Turk, R., Nguyen, H., Ross-Barta, S.E., Westra, S., et al. (2010). Distinct functions of glial and neuronal dystroglycan in the developing and adult mouse brain. J. Neurosci. *30*, 14560–14572. https://doi.org/10.1523/JNEUROSCI.3247-10.2010.

Sudo, A., Kanagawa, M., Kondo, M., Ito, C., Kobayashi, K., Endo, M., Minami, Y., Aiba, A., and Toda, T. (2018). Temporal requirement of dystroglycan glycosylation during brain development and rescue of severe cortical dysplasia via gene delivery in the fetal stage. Hum. Mol. Genet. *27*, 1174–1185. https://doi.org/10.1093/hmg/ddy032.

Suemori, H., Yasuchika, K., Hasegawa, K., Fujioka, T., Tsuneyoshi, N., and Nakatsuji, N. (2006). Efficient establishment of human embryonic stem cell lines and long-term maintenance with stable karyotype by enzymatic bulk passage. Biochem. Biophys. Res. Commun. *345*, 926–932. https://doi.org/10.1016/j.bbrc.2006.04.135.

Takahashi, K., Tanabe, K., Ohnuki, M., Narita, M., Ichisaka, T., Tomoda, K., and Yamanaka, S. (2007). Induction of pluripotent stem cells from adult human fibroblasts by defined factors. Cell *131*, 861–872. https://doi.org/10.1016/j.cell.2007.11.019.

Tanaka, A., Woltjen, K., Miyake, K., Hotta, A., Ikeya, M., Yamamoto, T., Nishino, T., Shoji, E., Sehara-Fujisawa, A., Manabe, Y., et al. (2013). Efficient and reproducible myogenic differentiation from human iPS cells: prospects for modeling Miyoshi Myopathy in vitro. PLoS One *8*, e61540. https://doi.org/10.1371/journal.pone.0061540.

Taniguchi-Ikeda, M., Kobayashi, K., Kanagawa, M., Yu, C.C., Mori, K., Oda, T., Kuga, A., Kurahashi, H., Akman, H.O., DiMauro, S., et al. (2011). Pathogenic exon-trapping by SVA retrotransposon and rescue in Fukuyama muscular dystrophy. Nature *478*, 127–131. https://doi.org/10.1038/nature10456.

Taniguchi-Ikeda, M., Morioka, I., Iijima, K., and Toda, T. (2016). Mechanistic aspects of the formation of alpha-dystroglycan and therapeutic research for the treatment of alpha-dystroglycanopathy: a review. Mol. Asp. Med. *51*, 115–124. https://doi.org/10.1016/j.mam.2016.07.003.

Uchimura, T., Otomo, J., Sato, M., and Sakurai, H. (2017). A human iPS cell myogenic differentiation system permitting high-throughput drug screening. Stem Cell Res. *25*, 98–106. https://doi.org/10.1016/j.scr.2017.10.023.

Wang, H. (2018). Modeling neurological diseases with human brain organoids. Front. Synaptic Neurosci. *10*, 15. https://doi.org/10.3389/fnsyn.2018.00015.

Watanabe, M., Buth, J.E., Vishlaghi, N., de la Torre-Ubieta, L., Taxidis, J., Khakh, B.S., Coppola, G., Pearson, C.A., Yamauchi, K., Gong, D., et al. (2017). Self-organized cerebral organoids with human-specific features predict effective drugs to Combat Zika virus infection. Cell Rep. *21*, 517–532. https://doi.org/10.1016/j.celrep.2017.09.047.

STAR★METHODS

KEY RESOURCES TABLE

REAGENT or RESOURCE	SOURCE	IDENTIFIER
Antibodies		
Alpha Dystroglycan(6A41)	Merck	Cat# 05-298, RRID:AB_309674
Alpha smooth muscle actin (alpha-SMA)	DAKO	Cat# M0851, RRID:AB_2313736
Beta dystroglycan(8D5)	Leica Biosystems	Cat# ab49515, RRID:AB_869400
$_{\beta}$-III-tubulin	Sigma	Cat# MAB1637, RRID:AB_2210524
Alpha Dystroglycan (IIH6)	SantaCruz	Cat# sc-53987, RRID:AB_831189
Forkhead box protein G1 (FOXG1)	Takara	Cat# M227, RRID:AB_2827749
COUP-TF-interacting protein 2 (Ctip2)	Abcam	Cat# ab18465, RRID:AB_2064130
Glial Fibrillary Acidic Protein (GFAP)	Merck	Cat# G3893, RRID:AB_477010
GFAP	Abcam	Cat# ab7260, RRID:AB_305808
Green Fluorescent Protein (GFP)	Abcam	Cat# ab13970, RRID:AB_300798
Laminin	Abcam	Cat# ab11575, RRID:AB_298179
Myosin Heavy Chain (MYH)	RSD	Cat# MAB4470, RRID:AB_1293549
Nanog	R&D	Cat# AF1997, RRID:AB_355097
Nestin	Abcam	Cat# ab22035, RRID:AB_446723
Nestin	BioLegend	Cat# 841901, RRID:AB_2565468
Neuronal nuclei (NeuN) (D4G40)	Cell Signalling	Cat# 24307, RRID:AB_2651140
Pax6	BioLegend	Cat# 901301, RRID:AB_2565003
Pax6	Abcam	Cat# ab78545, RRID:AB_1566562
Phosphorylated Vimentin (p-Vim)	MBL	Cat# D076-3, RRID:AB_592963
Polysialylated neural cell adhesion molecule (PSA-NCAM)	Millipore	Cat# MAB5324, RRID:AB_95211
Sox2	Abcam	Cat# ab97959, RRID:AB_2341193
Sox2	SantaCruz	Cat# sc-17320, RRID:AB_2286684
Sox17	R&D	Cat# AF1924, RRID:AB_355060
T-box, brain, 1(TBR1)	Abcam	Cat# ab31940, RRID:AB_2200219
T cell receptor alpha locus-1 (TRA1-60)	Sigma	Cat# MAB4360, RRID:AB_2119183
Primer sequences		
OCT3/4 (endo) hOCT3/4-S1165: 5′-GACAGGGGGAGGGGAGGAGCTAGG-3′	Takahashi et al. (2007)	N/A
OCT3/4 (endo) hOCT3/4-AS1283: 5′- CTTCCCTCCAACCAGTTGCCCCAAAC -3′	Takahashi et al. (2007)	N/A
SOX2 (endo) hSOX2-S1430 : 5′- GGGAAATGGGAGGGGTGCAAAAGAGG-3′	Takahashi et al. (2007)	N/A
SOX2 (endo) hSOX2-AS1555: 5′-TTGCGTGAGTGTGGATGGGATTGGTG-3′	Takahashi et al. (2007)	N/A
NANOG hNANOG forward : 5′-TGAACCTCAGCTACAAACAG-3′	Kim et al. (2009)	N/A
NANOG hNANOG reverse : 5′-TGGTGGTAGGAAGAGTAAAG-3′	Kim et al., (2009)	N/A
GAPDH GAPDH forward : 5′-ACCACAGTCCATGCCATCAC-3′	Okita et al. (2011)	N/A
GAPDH GAPDH reverse : 5′-TCCACCACCCTGTTGCTGTA-3′	Okita et al. (2011)	N/A
FKTN (total) human FKTN f1-F(exon5-6): 5′-TTGACAGGCCAGAGTTACAG-3′	this paper	N/A
FKTN (total) human FKTN f1-R(exon7) : 5′-GCCACAGCTTCCACAGTGTT-3′	this paper	N/A

(*Continued on next page*)

Continued

REAGENT or RESOURCE	SOURCE	IDENTIFIER
FKTN (normal) human FKTN : 5′-splf1TGTACCCTGTGAAACCCTCGAATAC-3′	Taniguchi-Ikeda et al. (2011)	N/A
FKTN (normal) human FKTN n rt-r3: 5′-TCTTGATGTCACTCAAAGTCTG-3′	Taniguchi-Ikeda et al. (2011)	N/A
FKTN (mis-spliced) human FKTN : 5′-splf1TGTACCCTGTGAAACCCTCGAATAC-3′	Taniguchi-Ikeda et al. (2011)	N/A
FKTN (mis-spliced) FCMDPIR : 5′-GAAAACCAGTGAGGCGTAGC-3′	Taniguchi-Ikeda et al. (2011)	N/A
FKTN genome-editing FKTN genome-edited f1 : 5′-TTCTCTCAAACAGCGTGCAG-3′	this paper	N/A
FKTN genome-editing FKTN genome-edited r1 : 5′-GGTGATACTGCAGTGCAAATG-3′	this paper	N/A
FKTN genome (intron 5) FKTNins5F1 : 5′-CATGTGCAAAAATTTATCTTTGGCTATCTC-3′	this paper	N/A
FKTN genome (intron 5) FKTNins5R1 : 5′-GGTCATTTTGAAAATATCGCTTGGTTCAG-3′	this paper	N/A
FKTN RNA (intron 5) RNAFKTNins5F1 : 5′-CATGCGATCCACTTGGTAGTC-3′	this paper	N/A
FKTN RNA (intron 5) RNAFKTNins5R1 : 5′-GGTACTGCTGAAAGAATGCTCG-3′	this paper	N/A
Single guide RNA FKTN-KO3 : 5′-TTGCACTGCAGTATCACCTATGG-3′	this paper	N/A

RESOURCE AVAILABILITY

Lead contact

Further information and requests should be directed by the Lead Contact, Mariko Taniguchi-Ikeda (mtani@fujita-hu.ac.jp).

Material availability

No unique materials were generated in this study.

Data code and availability

The data generated or analyzed in this study are available upon request from the Lead Contact, Mariko Taniguchi-Ikeda (mtani@fujita-hu.ac.jp).

EXPERIMENTAL MODEL AND SUBJECT DETAILS

Animals

All mouse experimental protocols were approved by the Ethics Review Committees for Animal Experimentation of Fujita Health University (AP18020-MD2). The mice used in the experiments (C57BL/6) were males between two and six months old. DMSO-solubilized D-Mn007 was injected either through the tail vein (n = 2) or intrathecally (n = 2), and then the mice were sacrificed 2 days after the injection. As a control, PBS alone was also injected through the tail vein (n = 2) or intrathecally (n = 2).

Ethical approval

The use of all clinical samples was approved by the Human Ethics Review Committees of the Fujita University (HG20-033) and the Kobe University Graduate School of Medicine (No. 1521).

Pluripotent stem cell culture

All research on human iPSCs and ESCs was approved by the Committee on Human Research and Stem Cell Research of the Fujita Health University and the Kobe University Graduate School of Medicine. All patient iPSC lines were generated and characterized using previously reported methods (Okita et al., 2011). In brief, 3 μg of an episomal expression plasmid mixture encoding OCT3/4, SOX2, KLF4, EBNA1, and shRNA for TP53 (Okita et al., 2011) was electroporated into 3×10^6 lymphoblasts with a Nucleofector electroporation device (Lonza, Allendale, NJ, USA) according to the manufacturer's instructions (electroporation program V024). Cells were detached within 1 week of electroporation and seeded at $1–30 \times 10^4$ cells per well of a 6-well dish onto irradiated or mitomycin-C treated SNL feeder cells (Suemori et al., 2006). The culture medium was replaced the

next day with StemSpan-ACF (Stem Cell Technologies, Vancouver, CANADA). Colonies were counted approximately 10 days after electroporation, and colonies similar in shape to hESCs were selected for further cultivation and evaluation. Established human iPSC lines were cultured in DMEM/F12 GlutaMAX medium (Thermo Fischer Scientific, MA, USA) containing 20% KnockOut Serum Replacement (Thermo Fischer Scientific), 1% non-essential amino acids (Thermo Fischer Scientific), 0.1 mM β-mercaptoethanol (Thermo Fischer Scientific), 1% ampicillin-streptomycin (Sigma-Aldrich, St Louis, USA), and basic fibroblast growth factor (bFGF) on SNL feeder cells. Collagenase type IV (Sigma-Aldrich), trypsin (Thermo Fischer Scientific), or the STEMPro EZ Passage Tool (Theromo Fischer Scientific) were used for cell passaging.

Chromosomal analysis of patient iPSCs was performed with a commercial test (SRL, Tokyo, Japan). The validated iPSC line 201B7 was purchased from the Riken Cell Bank (Tsukuba, Japan). Validated hESCs (KhES-1) were purchased from Kyoto University (Kyoto, Japan) and maintained on a feeder layer of mouse embryonic fibroblasts.

Embryoid body-mediated *in vitro* spontaneous differentiation

In vitro embryoid body formation was performed based on a previously published protocol (Takahashi et al., 2007). In brief, undifferentiated iPSC clones were treated with Dissociation Solution for Human ES/iPS Cells (CTK solution; REPROCELL, Kanagawa, Japan), transferred onto nonadherent poly-HEMA (Merck, Darmstadt, Germany)-coated dishes, and cultured in Primate ES Medium (REPROCELL, Yokohama, Japan) without bFGF for 7 days. The resulting embryoid bodies were plated onto gelatin-coated plates and cultured in the same medium for another 7 days. The differentiated cells were immunostained as described below.

METHOD DETAILS

Sequencing of patient genomic DNA and RNA

Patient genomic DNA from peripheral blood and iPSCs was extracted using the Qiagen Blood Mini Kit (Qiagen, Hilden, Germany). RNA from iPSCs was extracted using an RNeasy Mini Kit (Qiagen). Extracted patient genomic DNA was amplified using previously reported polymerase chain reaction (PCR) primers, while RNA was reverse-transcribed using SuperScript III Reverse Transcriptase with random primers (Invitrogen, Waltham, Massachusetts, USA), and sequencing was performed using previously reported methods (Kobayashi et al., 2017).

Cerebral organoid generation and culture

Cerebral organoids were generated according to previously published methods (Kadoshima et al., 2013; Watanabe et al., 2017). In brief, iPSCs (FCMD patient-derived iPSCs FK15 and FK17 and the healthy control clone 201B7) or hESCs (the healthy control clone KhES-1) were dissociated into single cells and reaggregated in low-attachment 96-well V-bottom plates (Sumitomo Bakelite, Tokyo, Japan) with cortical differentiation medium (described below) at a density of 9,000 cells per aggregate in 100 μL per well. Cortical differentiation medium consisted of: Glasgow-MEM, 20% KnockOut Serum Replacement, 0.1 mM Non-Essential Amino Acids (Thermo Fischer Scientific), 1 mM sodium pyruvate, 0.1 mM β-mercaptoethanol, 100 U/mL primocin (InvivoGen, San Diego, USA), the rho kinase inhibitor Y-27632 (20 μM, days 0–6), the WNT inhibitor IWR1-ε (Merck, 6 μM, days 0–18), and the TGF-β inhibitor SB431542 (Tocris, 10 μM, days 0–18). The medium was changed every 3 days until day 18. On day 18, the aggregates were transferred to ultra-low adhesion plates and cultured in DMEM/F12 medium with 1% GlutaMAX, 1% N-2 Supplement (Thermo Fischer Scientific), chemically defined lipid concentrate (CDLC; Gibco), 100 μg/mL primocin, and 0.4% methylcellulose (Sigma) and grown in 40% O_2/5% CO_2. On day 35, the medium was changed to N2B27 medium containing DMEM/F12 with GlutaMAX, N2, CDLC, 0.4% methylcellulose, B27 without vitamin A (Invitrogen), 1% Growth Factor Reduced Matrigel (Thermo Fisher Scientific), 5 μg/mL heparin (Sigma), and 2,000 U/mL leukemia inhibitory factor (Merck). Organoids were subsequently halved every 2 weeks to prevent attachment between them and routinely sustained for up to 150 days. Organoids were processed for immunohistochemical analyses. Organoid size was quantified from microscopic pictures of 20 organoids at 3 and 5 weeks with ImageJ software (https://imagej.nih.gov/ij/). The two-group comparisons of the size of the organoids (Figure 3A) were performed using the Mann-Whitney U test.

Myogenic differentiation of pluripotent stem cells

For MyoD-mediated myogenic differentiation, tetracycline-inducible MyoD expression piggyBac vector KW879-hMyoD (Uchimura et al., 2017) were transfected into both 201B7 and FK17. After puromycin selection, myogenic differentiation was conducted as previously described (Uchimura et al., 2017).

Semi-quantitative and real-time quantitative RT-PCR

For Figure 1F, total RNA was isolated using TRIzol (Thermo Fischer Scientific) and treated with the TURBO DNA-free kit (Thermo Fisher Scientific). The PrimeScript II 1st Strand cDNA Synthesis Kit (Takara, Kyoto, Japan) was used to synthesize cDNA from 125 ng of total RNA. The resulting cDNA was subjected to semi-quantitative RT-PCR with the Takara Ex Taq PCR kit (Takara). Primer sequences were listed in Table S1.

Chemical compound

Mn007 was synthesized by Nard Institute, Ltd. (Amagasaki, Hyogo, Japan) and reconstituted in DMSO. Dansyl-conjugated Mn007 was synthesized as follows: 46 mg (0.1 mmol) of Mn007 and 50 μL of trimethylamine (Fujifilm Wako Pure Chemical, Miyazaki, Japan) were dissolved in 5 mL of tetrahydrofuran (THF), then 35 mg (0.13 mmol) of dansyl chloride (Tokyo Chemical Industry, Tokyo, Japan) was added, and the solution was stirred at 25 °C for 3 h. Dansyl-conjugated Mn007 was purified using high-performance liquid chromatography (LC-20AT, Shimadzu, Kyoto, Japan) equipped with an ODS column (10 × 250 mm, GL Science, Tokyo, Japan). To generate rhodamine-conjugated Mn007, Mn007 (10 mg, 0.02 mmol) was dissolved in 5 ml dichloromethane containing 0.05 ml pyridine. Rhodamine B isothiocyanate (107 mg, 0.2 mmol) was added to the dichloromethane solution, followed by gentle stirring at 25°C overnight. After the reaction, Mannan007 conjugated with rhodamine B was purified using an HPLC system equipped with an ODS column.

Immunofluorescence and western blotting

Human iPSCs were fixed for immunofluorescence analyses with PBS containing 4% paraformaldehyde (PFA; WAKO, Osaka, Japan) for 10 min at room temperature. After washing the cells with PBS, blocking was performed with PBS containing 5% normal donkey serum (Abcam, Cambridge, UK), 1% BSA (WAKO), and 0.1% Triton X-100 (Merck) for 45 min at room temperature. Primary antibodies included those against NANOG, SOX2, TRA1-60, β-III-tubulin, αSMA, and SOX17 (Table S2). The secondary antibody used for NANOG and SOX17 was Alexa Fluor 488-conjugated anti-goat IgG (1:500; Invitrogen), for TRA1-60 was Alexa Fluor 488-conjugated anti-mouse IgG (1:500; Invitrogen), for β-III-tubulin and α-SMA was Alexa Fluor 594-conjugated anti-mouse IgG (1:500; Invitrogen), and for SOX2 was Alexa Fluor 594-conjugated anti-rabbit IgG (1:500; Invitrogen). Nuclei were stained with 1 μg/mL Hoechst 33342 (Thermo Fisher Scientific).

Organoids were fixed for Immunofluoroscence analysis with 4% PFA in PBS for 20 to 40 min depending on the size of the organoid, washed with PBS, dehydrated with 30% sucrose in PBS for 2 h at 4 °C, embedded in blocks of Optimal Cutting Temperature compound, and frozen on dried ice. Cryosections (10 μm) were analyzed by Immunofluorescence. Permeabilization was performed for 20 min with 0.1% Triton X-100 in PBS, and blocking was performed for 1 h with 10% donkey serum and 0.1% Triton X-100 in PBS. All antibodies used to for organoid tissue and western blotting are listed in Table S2. Primary antibody incubations were performed at 4 °C overnight, and secondary antibody incubations were performed at room temperature for 1 h. After primary and secondary antibody incubations, three 5-min washes in PBS were performed. The secondary antibodies were raised in donkey; conjugated with either Alexa Fluor 488, Cy3, or Cy5; and were directed against goat, rabbit, rat, or mouse IgG or mouse IgM (all used at 1:500 dilution; Jackson ImmunoResearch, PA, USA). The laminin clustering assay and western blotting were performed as described previously (Taniguchi-Ikeda et al., 2011). For staining of glycosylated αDG, neither Triton X-100 nor Tween 20 were used in order to avoid the washing out of glycans. In brief, plates were dried for 2 min, fixed with 4% PFA for 1 min, washed with 50% acetone for 1 min, and then blocked with 10% donkey serum in PBS without Triton X-100. Nuclei were stained with 1 μg/mL 4′,6-diamidino-2-phenylindole (DAPI, Dojindo, Kumamoto, Japan).

CRISPR/Cas9 knockout of *FKTN* in HEK cells

The CAS9 protein and CRISPR RNA were electroporated into HEK cells (BioWhittaker, Walkersville, MD, USA) using a NEPA21 Super Electroporator (Nepa Gene, Chiba, Japan) following the manufacturer's instructions. Single-cell clones were expanded then passaged twice before αDG-negative cells were sorted using a MoFlo cell sorter (Beckman Coulter, Brea, CA, USA). For staining, cells were first blocked with an FcR Blocking Reagent (1:200 dilution) for 20 minutes (Miltenyi Biotec, Bergisch Gladbach, Germany) then incubated for 30 min with an anti-αDG antibody (clone: IIH6, 1:50; Millipore), washed with PBS, and incubated with an Alexa Fluor 647-conjugated anti-mouse IgM (1:50; BioLegend, San Diego, CA, USA). After sorting, the FKTN gene was sequenced in several single-cell clones to check for insertions and

deletions. One clone showed insertions and deletions in both alleles (Figure S2, the second sequence). To verify the sequence of each allele of this clone, we ligated PCR products into a plasmid vector (TOPO® TA Cloning Kit for sequencing, Thermo Fisher) then transformed E-coli with the plasmid and checked the sequences from each colony. Chronographs were visualized with Geneious Prime (Biomatters, Ltd.Auckland, New Zealand). The clone possessed a 7 bp deletion/1 bp insertion on one allele and a 6 bp deletion in the other allele (Figure S2, the third and fourth sequences). Based on western blotting, this clone lacked αDG glycosylation (Figure 2C).

Migration assay

The EF1.PGK.GFP plasmid vector (Addgene, MA, USA) was used to label glial progenitors. In brief, Microcap pre-pulled glass needles (Drummond Scientific Company, Broomall, PA, USA) were inserted into the rosette structures of cortical organoids between day 56 and 60, and the plasmid solution (1 μl, 1 μg/μL) was injected into the ventricle. The organoids were then placed into an electroporation glass chamber with Opti-MEM to achieve equal current and immediately electroporated (conditions: 5 pulses, 125 V, 50 ms duration, and 1 s intervals using a NEPA21 Super Electroporator). Organoids were then put back into the incubator and checked 24 h, 48 h, and 1 week later and then fixed and stained as described above.

QUANTIFICATION AND STATISTICAL ANALYSIS

Because normality cannot be guaranteed for all continuous values, the Mann-Whitney U test was used to test for differences between two groups (FCMD vs. normal control). Fisher's exact test was used for the comparison of categorical data. Two-sided p values of <0.05 were considered statistically significant. All analyses were performed using R version 4.1.0 (www.r-project.org).